IEEE Photonics Journal
An IEEE Photonics Society Publication

Improved Performance of Nanohole Surface Plasmon Resonance Sensors by the Integrated Response Method

Volume 3, Number 3, June 2011

Mandira Das
Donna Hohertz
Rajinder Nirwan
Alexandre G. Brolo
Karen L. Kavanagh
Reuven Gordon

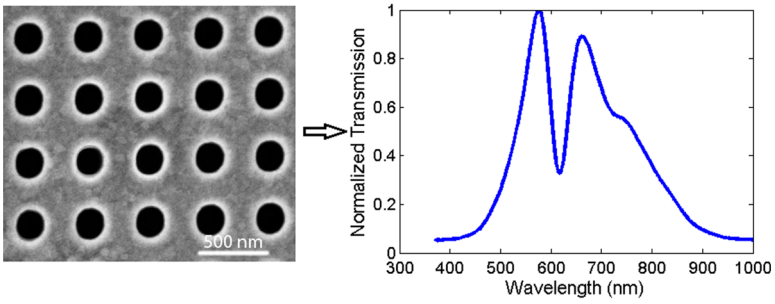

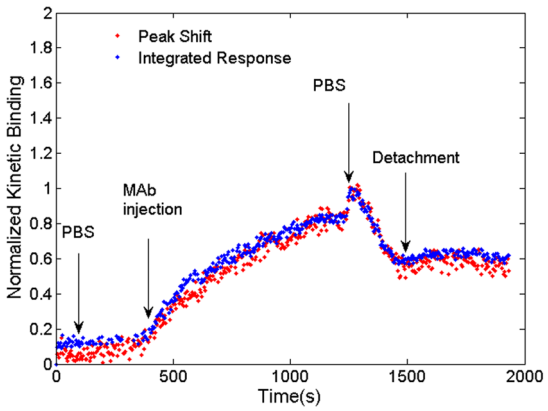

DOI: 10.1109/JPHOT.2011.2143702
1943-0655/$26.00 ©2011 IEEE

Improved Performance of Nanohole Surface Plasmon Resonance Sensors by the Integrated Response Method

Mandira Das,[1] Donna Hohertz,[2] Rajinder Nirwan,[3] Alexandre G. Brolo,[3] Karen L. Kavanagh,[2] and Reuven Gordon[1]

[1]Department of Electrical and Computer Engineering, University of Victoria, Victoria, BC V8W 3P6, Canada
[2]Department of Physics, Simon Fraser University, Burnaby, BC V5A 1S6, Canada
[3]Department of Chemistry, University of Victoria, Victoria, BC V8W 3V6, Canada

DOI: 10.1109/JPHOT.2011.2143702
1943-0655/$26.00 ©2011 IEEE

Manuscript received February 17, 2011; revised April 7, 2011; accepted April 8, 2011. Date of publication April 19, 2011; date of current version May 13, 2011. This work was supported by the Natural Science and Engineering Research Council of Canada. Corresponding author: R. Gordon (e-mail: rgordon@uvic.ca).

Abstract: We examine both experimental and simulated data of the optical transmission response of nanohole arrays in metal films to bulk and surface refractive index changes. We compare the signal-to-noise performance of the following three different analysis methods: the conventional peak shift method, a normalized-difference integrated-response method that is commonly used in 3-D plasmonic crystals, and an integrated response (IR) method. Our IR method shows a 40% and 90% improvement in the signal-to-noise ratio (SNR) for bulk and surface binding tests, respectively, compared with the direct measurement of the transmission-peak wavelength shift, promising improved sensing performance for future nanohole-array sensor applications.

Index Terms: Plasmonics, biosensors.

1. Introduction

Surface plasmon resonance (SPR) sensors are widely used for label-free sensing in biomedical applications, ranging from drug discovery [1] to gene identification [2]. SPR is sensitive to surface binding due to the decaying evanescent field of surface plasmons (SPs). SPs are electromagnetic modes that propagate at a metal-dielectric interface. The propagation constant (wave vector) of a SP on a semi-infinite planar boundary between a metal and a dielectric depends on the refractive index of the dielectric medium [3]. This property of SPs is used to measure bulk and surface refractive index changes.

The direct excitation of SPs from a smooth metallic surface is not possible due to the momentum mismatch. Therefore, to excite SPs, a coupling mechanism is required, such as attenuated total reflection using a prism [4] or diffraction on periodic metallic gratings [5]–[7]. One such approach utilizes the Bragg (grating) resonances of periodically arranged, subwavelength nanoholes in metal films. The optical transmission properties of such arrays has generated considerable interest since Ebbesen *et al.* demonstrated that subwavelength hole arrays have large intensity transmission resonances [8] associated with the excitation of SPs by the periodic holes [9]. This discovery encouraged researchers to explore the potential for creating nanoscale sensors [10]–[24] due to the nanohole array's simple collinear geometry, and potential for dense integration. The biochemically

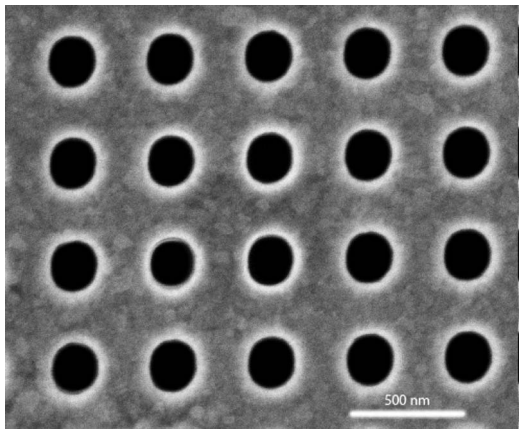

Fig. 1. Scanning electron microscope picture of a focus-ion-beam milled nanohole array with 200 nm hole diameter and 450 nm periodicity.

functionalized nanohole arrays offer a new strategy for parallel detection of chemical and biological agents [24].

Signal information from SPR sensors is extracted using various analysis methods. For Kretschmann SPR (prism coupling), the sensing is typically based on localizing and tracking the minimum in the SPR reflectivity spectrum (wavelength or angular). This is achieved via several different methods, such as fitting the spectra with a polynomial of order 2–7 or a Lorentzian curve (with or without a linear term) [23]; optimal linear data analysis [25], centroid localization and tracking [4]; model parameterization and linear projection [26]; and locally weighted parametric regression [27]. Similarly, in nanohole array SPR, one tracks the location of the transmission resonance peak; however, monitoring only the peak position ignores significant information present in the entirety of the wavelength (or angular) spectrum. In 3-D plasmonic crystals, the complex wavelength transmission spectrum showed an improved sensitivity when analyzed with a normalized-difference integrated-response (NDIR) over the entire transmission spectrum [28].

In this work, we apply the integrated response (IR) analysis method to the transmission spectra of nanohole arrays in metal films while monitoring both the sensitivity and noise performance. We examine the bulk refractive index response using both experimental measurements and simulated idealized finite-difference time-domain (FDTD) computations with added noise. Additionally, we assess the surface response using experimental surface binding data. We demonstrate improved sensing characteristics for our IR method as compared with the peak shift or the NDIR method.

2. Experimental Methods

2.1. Nanohole Array Fabrication

Fig. 1 shows an array of circular nanoscale holes (200 nm diameter, 450 nm periodicity) milled in a thermally evaporated gold (100 nm)/titanium (5 nm) film on a glass slide $(1 \times 1 \times 0.04$ in$)$. A focused ion beam (FIB) (FEI 235 dual-beam, 30 keV, 2.2 μA emission current with 30 pA aperture), was used to mill square arrays each having a surface area of 20 μm^2.

2.2. Bulk Refractive Index Measurements

A slide containing nine gold arrays was cleaned in an aqueous acid and peroxide mixture (H_2SO_4 and H_2O_2) then exposed to varying concentrations of aqueous glucose solutions. To measure the transmission intensity spectra, it was placed on the stage of an inverted optical microscope (Reichert #325098). White light (Fiber-Lite Series 180) focused through an objective lens (25$\times$) was used to illuminate a single nanohole array. The transmitted light was collected by a fiber optic cable connected to a computer-controlled spectrometer (Photon Control SPM-002,

SPECSOFT, ver. 2.3.4.4). We collected transmission, background (transmission through a pinhole), reference (transmission response of water), and dark noise (light input off) intensity spectra. Each collected spectrum was the average of 100 individual measurements of 1 s exposures (200 nm to 1090 nm, 3166 data points). The spectral resolution is between 0.8 and 2 nm over the wavelength range. Each spectrum was smoothed using a boxcar of five. Measurements were repeated five times under identical experimental conditions.

2.3. Surface Binding Experiments

Surface binding experiments were conducted to determine the applicability of the IR analysis method for the detection of surface refractive index changes. The affect on transmission of binding of a particular monoclonal antibody (MAb), i.e., 17-9, to the nanohole array functionalized with the corresponding antigen (Ag), the hemagglutinin (HA) peptide was monitored. The gold surface was functionalized with HA Ag by a series of surface modification steps. First, it was soaked overnight in a biotin-polyethylene glycol-thiol, (1 mM, HS-$(CH_2)_{11}$-$(OCH_2CH_2)_6$-NH-Biotin) ethanol solution, which created a self-assembled monolayer. The slide was then soaked in a streptavidin phosphate buffered saline (PBS) (2 hr, 100 μg/mL, PBS) followed by a biotinylated HA Ag solution (2 hr, 25 μg/mL). Transmission spectra were collected from each array between each step to monitor the modification process. The affinity of the MAb to the Ag was monitored using the nanohole arrays integrated in a microfluidic setup equipped with a syringe pump (NE 1800 New Era Pump Systems Inc.). The binding kinetics of the 17-9 MAb (10 μg/mL in PBS, flow rate 5 μL/min,14 min) to the HA Ag was monitored in real time via changes in collected optical spectra (every 4 s). A baseline reference was established using an array with a blank solution without MAb. The detachment kinetics of the MAb were observed by switching to the blank solution after binding was complete. PBS solution was flowed through again to observe the detachment of the MAb.

2.4. Simulations

We conducted simulations of the optical experiments using FDTD calculations. A plane-wave light source at normal incidence was used to excite the nanohole array. Periodic boundary conditions on both in-plane *x*- and *y*-axes (each parallel to the array edge) were used with perfectly matched layer (PML) boundary conditions along the perpendicular *z*-axis. A mesh-override grid size of 1.8 nm ensured accurate modeling of the plasmonic effects of the metal (as verified by convergence tests). The transmission was monitored at a plane 50 nm from the surface of the metal film on the glass side.

Since the experiments operate at relatively high optical intensities, shot noise should dominate over other noise contributions, such as intensity noise of the source and thermal and read-out noise of the detector. Therefore, only shot noise, which varies as the square root of the intensity, was added to the simulated spectrum. To obtain five repeated spectra similar to the real experiment, five independent, normally distributed, random noise quantities were used that generated a standard deviation of 0.15 (using the rand function in MATLAB).

3. Methods of Analysis

Our proposed IR analysis of the transmission spectra of nanohole arrays for biosensing applications uses the square root of the integrated mean-squared variation of the spectrum over the entire wavelength range. The mathematical expression is as follows:

$$IR = \sqrt{\int_{\lambda_1}^{\lambda_2} \left| D(\lambda)^2 - \overline{D(\lambda)^2} \right| d\lambda} \tag{1}$$

where IR is the integrated response, $D(\lambda) = S_{\text{ref}}(\lambda) - S(\lambda)$ is the difference in the signal between the reference spectrum, $S_{\text{ref}}(\lambda)$, and the measured signal $S(\lambda)$, and $\overline{D}(\lambda)$ is the average of the difference signal over the entire spectrum.

Our evaluation considers predominantly the signal-to-noise ratio (SNR) to evaluate sensitivity and noise performance without disrupting the linear response found with the peak shift curve. The noise is defined as the standard deviation of the IR from five repeated spectra.

Undesirable nonlinearity appeared in SNR curves when integrating higher powers (of order 2, 3, and 4) of the difference signal $D(\lambda)$ using (2):

$$\text{IR} = \int_{\lambda_1}^{\lambda_2} |D(\lambda)|^n \, d\lambda \tag{2}$$

where $n = 2, 3, 4, 5$. Therefore, we consider only the case represented by (1).

In addition, we compare the IR method to recently described work with 3-D plasmonic crystal templates, which uses an IR based on the normalized difference expressed as follows [28]:

$$\text{NDIR} = \int_{\lambda_1}^{\lambda_2} \left| \frac{S_{\text{ref}}(\lambda) - S(\lambda)}{S_{\text{ref}}(\lambda)} \right| d\lambda \tag{3}$$

We also reproduced surface binding curves as a function of time with this method to observe how they fit to the peak-shift response curve.

The IR method was also compared with the peak shift response method. The peak was found by fitting the curves using a polynomial fit (order 4, over range 20 nm about the peak). The peak was tracked by tracking the maximum point based on the polynomial fit.

Peak shift $\text{PS} = |P_{ref}(\lambda) - P(\lambda)|$, where $P_{ref}\ (\lambda)$ is the peak wavelength of the reference signal, and $P(\lambda)$ is the signal with a change in the refractive index. The noise in the NDIR and PS is defined as the standard deviation of five repeated tests under identical experimental conditions. We have also used a different definition of the noise as the simple point-by-point absolute difference between two different spectra (i.e., one repeated test). For that method, we saw similar results; however, the present method is chosen since it contains statistics over a greater number of repeated tests.

4. Results

4.1. Bulk Refractive Index Sensing

Fig. 2(a) shows the spectra of the source. Fig. 2(b) shows the experimental transmission spectrum of a periodic circular-hole array for different concentrations of aqueous glucose solutions over the hole array. The reference spectra are the response in water. Fig. 2(c) shows the FDTD simulations of the transmission spectra for the same structures as measured in Fig. 2(b) for different refractive index solutions. A refractive index of 1.3538 corresponds to a glucose concentration of 1 M [29]. Both the experimental and simulated spectra have two major peaks, in the ranges 570–610 nm and 680–710 nm. We attribute the peaks to the Bragg resonance-enhanced transmission at the glass and solution interfaces (as modified by the SP dispersion [9]). The peak at 680 nm is (1,0) Bragg resonances associated with the glass interface (the shoulder peak at 650 nm arises due to the Wood's anomaly minimum at 670 nm). The peak at 600 nm corresponds to the (1,0) Bragg resonance off the solution interface. The peak at 570 nm is attributed to the (1,1) resonance of the glass interface. The simulated and the experimental results differ for a number of reasons, including the finite collection aperture of the experiments, the finite extent of the arrays, nanohole tapering and edge smoothing produced during FIB milling, and nonnormal incidence from the sources. The main point of the FDTD simulations, however, was to present an idealized case that is free from experimental imperfection, and in this regard, we have shown the relative performance of the different approaches. It was not our intention to reproduce exactly the results of the experiment with the FDTD, although reasonable qualitative agreement is seen.

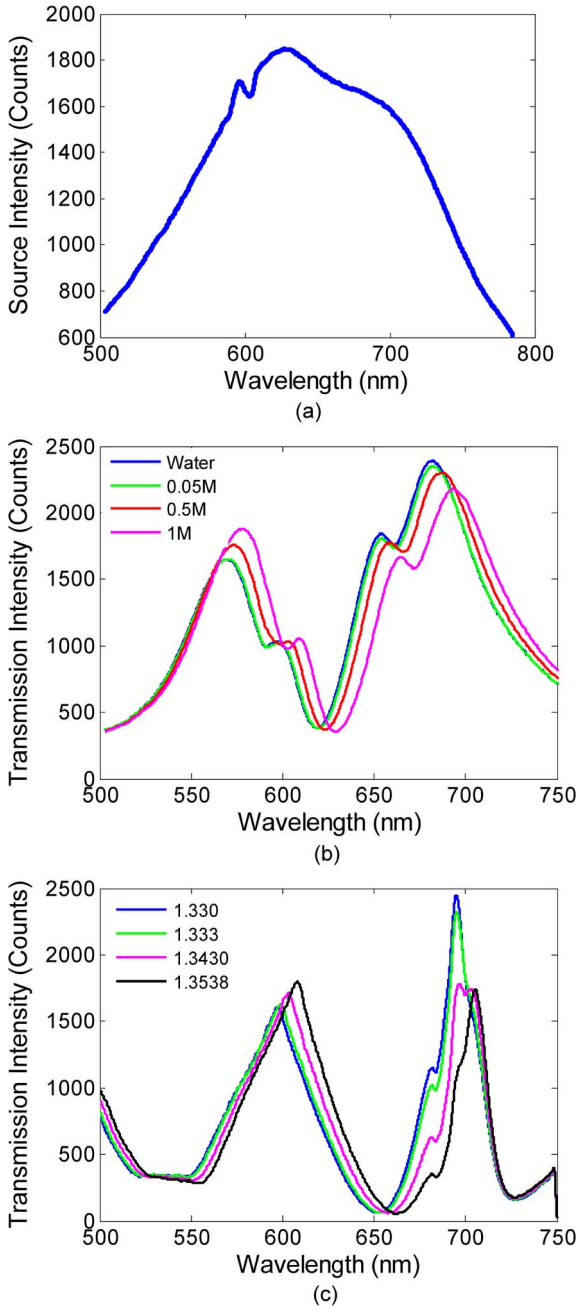

Fig. 2. (a) Source spectrum of a computer-controlled spectrometer (Photon Control SPM-002, SPECSOFT, ver. 2.3.4.4). (b) Transmission spectra through a hole array of 200 nm diameter round holes with 450 nm periodicity in a 100 nm thick layer of gold on Cr coated glass substrate. The different curves refer to transmission in different concentrations of glucose, 0.05 M (green), 0.5 M (red), and 1 M (magenta). The water spectrum (blue) is the reference. (c) FDTD simulation spectra of a hole array consisting of 200 nm diameter round holes at 450 nm periodicity on a 100 nm thick gold film on Cr-coated glass. The different curves are due to the change in the bulk refractive index of 1.3300 (blue), 1.3330 (green), 1.3430 (magenta), and 1.3538 (black) in the aqueous medium. The blue curve is taken as the reference.

Fig. 3(a) shows the SNR performance as calculated from the experimental data, using the three different analysis methods: IR, NDIR, and PS. The IR and NDIR analysis was applied to a spectral range of 500–750 nm as only this wavelength range shows significant spectral features. The peak

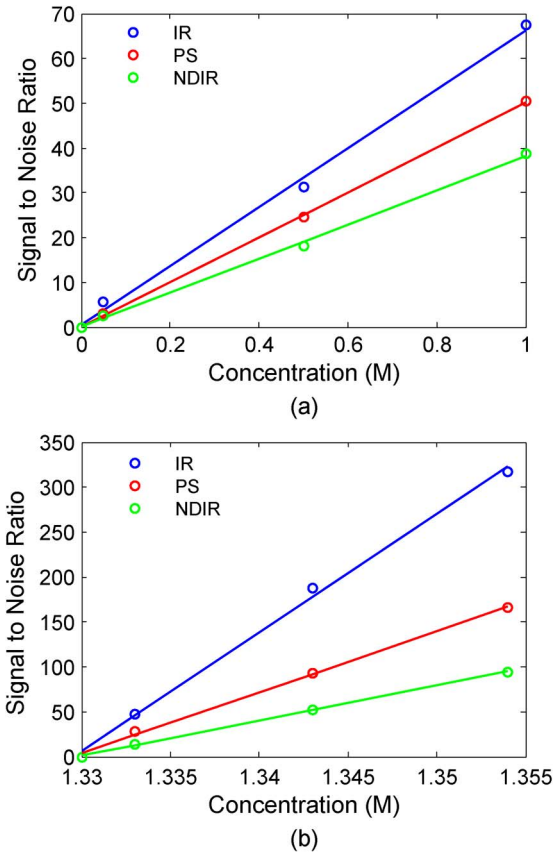

Fig. 3. Variation of signal to noise ratio with (a) glucose concentration using experimental data and (b) with refractive index using FDTD simulated data. The integrated response (IR) (blue) shows a higher sensitivity compared with the peak shift (PS) (red) and the normalized difference integrated response (NDIR) (green) method.

positions were obtained by using a polynomial (order 4) curve-fitting technique. The data shows a higher SNR for the IR method, as compared with the PS and NDIR methods. Fig. 3(b) shows the calculated SNR from simulated data again using the IR, PS, and NDIR methods. Comparing Fig. 3(a) and (b), the IR method is superior to the PS and NDIR methods in both real and simulated experiments.

4.2. Surface Sensing

Fig. 4(a) shows the normalized transmission spectra before (1 s) and after (1200 s) binding occurs. Fig. 4(b) is a zoomed version of Fig. 4(a). It shows the shift in the two curves more clearly. Fig. 4(c) depicts the normalized response of the PS and IR method as a function of time for the surface sensing experiment. At 400 s, 10 μg/mL MAb was injected for 14 min (as seen from the sharp increase in the signal). The refractive index change in this portion of the curve reflects the dynamics of the surface and bulk. To evaluate the net surface binding, the surface was washed with a PBS solution at 1200 s. After the wash, the response dropped to a certain value at 1500 s. This represents the absorbed MAb on the surface.

The observed reaction rate k_{obs} for the absorption of 10 μg/mL 17/9 MAb was calculated from an exponential fitting and was determined to be $1.8 \times 10^{-3} \pm 3 \times 10^{-4}$ s^{-1}. A separate k_{obs} was determined from a different concentration of 17/9 MAb, and the observed reaction rate values were used to obtain an estimate of magnitude for the k_{on} $(2 \times 10^3$ s^{-1}M$^{-1})$ and the k_{off} $(6 \times 10^{-4}$ s$^{-1})$.

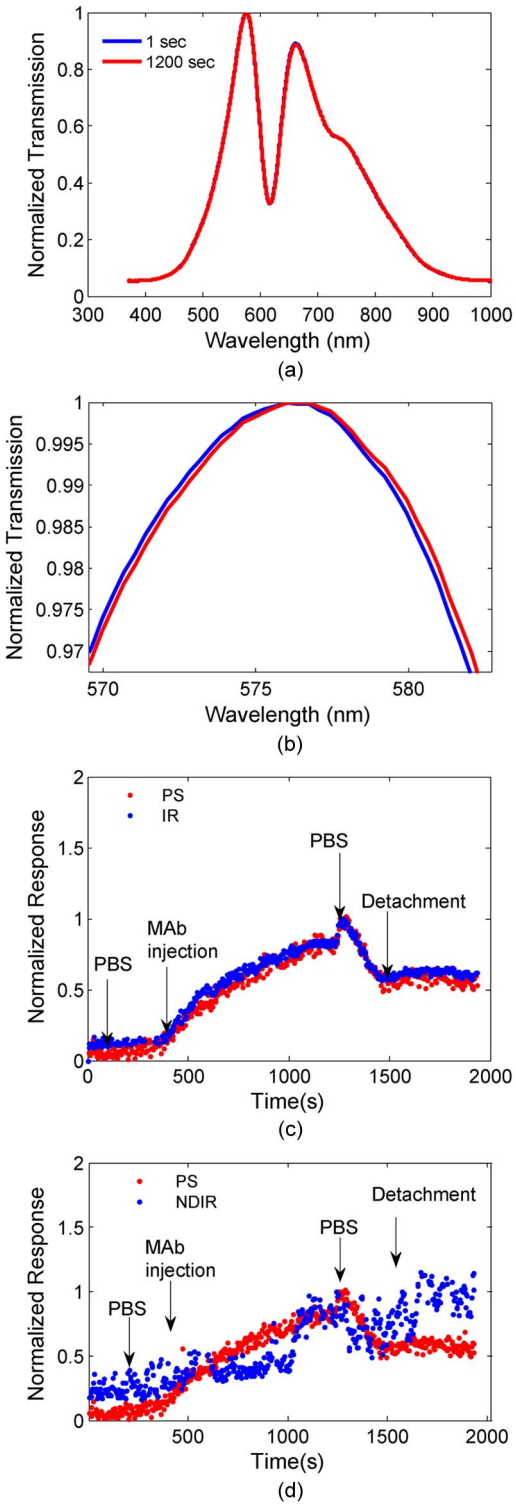

Fig. 4. (a) Normalized transmission spectra of binding test before (1 s) and after (1200 s) binding. (b) A zoomed version of (a) to show the spectral shift in the curves at 1 s and 1200 s. (c) Comparison of noise performance in a kinetic curve of monoclonal antibody (MAb) solution (10 μg/mL) binding to antigen (Ag) using PS response (red) and IR method (blue) and (d) comparison of noise performance in a kinetic curve of monoclonal antibody (MAb) solution (10 μg/mL) binding to antigen (Ag) using PS response (red) and NDIR method (green). For better comparison, the curves are normalized to a baseline so that they overlap.

The noise in the surface sensing is defined as the steady-state standard deviation of the peak shift points for peak shift noise and as the steady-state standard deviation of the IR points for IR noise. The first peak in the 575 nm wavelength region is tracked. Fig. 4(d) compares the results of the PS and NDIR method. The binding curves for this method showed more noise than the IR method and gave a response which does not follow the general trend of the peak shift response binding curve. The IR method demonstrates an improvement (i.e., reduction) of noise in kinetic binding curves, as compared with both the PS and NDIR methods. The IR method retains the general shape of the binding curve [see Fig. 4(c)]; however, distortion is observed in the NDIR analysis [see Fig. 4(d)].

5. Discussion

The IR method demonstrates better SNR performance as compared with the PS and NDIR methods for both experimental and simulated experiments of bulk refractive index variations. Additionally, this method exhibits similar performance improvement when applied to surface binding experiments.

By definition, a sensitivity improvement is an increase in the slope of the SNR curve. In the case of bulk refractive index experiments, the improvement is 1.4 ± 0.1 times and 1.8 ± 0.1 times that of the PS and NDIR methods, respectively. This is an improvement of 40% over the conventional peak shift method. The results for the corresponding simulated analysis shows a 1.7 ± 0.1 and 3.1 ± 0.1 times improvement relative to the peak shift and the NDIR, respectively. The IR performance is 70% better than the peak shift method in this idealized case. For all cases, the curves maintain linearity, and the IR shows the best performance. In the surface binding experiment, the noise level decreases from 0.0964 to 0.0053, resulting in a 90% improvement, as compared with the peak shift response. Additionally, the response curve shape is maintained. The NDIR for surface binding altered the curve shape and demonstrated an inferior noise performance.

The improvement found in the IR method results from additional information contained in the transmission response over the entire spectrum and due to lower noise (as random noise values are integrated over a range). Although the NDIR is similar to the IR method, the distortions in the NDIR analysis arise from the term in the denominator in (3). The analysis is highly dependent on the reference signal itself. Where the signal is small, the response is large, even though the information contained in that part of the spectra may be limited. The IR method is of particular interest for situations where there is a complex transmission spectrum. This is the case, for instance, in experiments using large area periodicity arrays fabricated using high-throughput photolithographic techniques [30]. The IR method can also be extended to hyperspectral imaging [31].

6. Conclusion

We have shown the analysis for optical transmission response of nanohole arrays in metal films subjected to bulk and surface refractive index changes using a square-root integrated mean-difference-squared method. Our analysis shows a 40% improvement in sensitivity for the bulk sensing experiment and a 90% improvement in noise for the surface sensing experiment compared with the conventional peak wavelength shift method and even better compared with the NDIR method. This IR method provides better performance because it reduces the noise by incorporating the information contained in the entire optical spectrum, while not distorting the response, as compared with the peak-shift method. Future plans include employing this method to large period structures with complex wavelength spectra.

Acknowledgment

The authors thank Dr. J. Scott and Dr. N. Gulzar for supplying antibodies used in the surface binding experiments and Dr. B. Gray and S. Romanuik for microfluidics consultations.

References

[1] M. A. Cooper, "Optical biosensors in drug discovery," *Nat. Rev. Drug Discov.*, vol. 1, no. 7, pp. 515–528, Jul. 2002.
[2] W. Jin, X. Lin, S. Lv, Y. Zhang, Q. Jin, and Y. Mu, "A DNA sensor based on surface plasmon resonance for apoptosis associated genes detection," *Biosens. Bioelectron.*, vol. 24, no. 5, pp. 1266–1269, Jan. 2009.
[3] J. Homola, "Present and future of surface plasmon resonance biosensors," *Anal. Bioanal. Chem.*, vol. 377, no. 3, pp. 528–539, Oct. 2003.
[4] G. G. Nenninger, M. Piliarik, and J. Homola, "Data analysis for optical sensors based on spectroscopy of surface plasmons," *Meas. Sci. Technol.*, vol. 13, no. 12, pp. 2038–2046, Dec. 2002.
[5] J. Dostálek and J. Homola, "Surface plasmon resonance sensor based on an array of diffraction gratings for highly parallelized observation of biomolecular interactions," *Sens. Actuators B, Chem.*, vol. 129, no. 1, pp. 303–310, Jan. 2008.
[6] E. K. Popov, N. Bonod, and S. Enoch, "Comparison of plasmon surface waves on shallow and deep metallic 1D and 2D gratings," *Opt. Express*, vol. 15, no. 7, pp. 4224–4237, Apr. 2007.
[7] C. J. Alleyne, A. G. Kirk, R. C. McPhedran, N. A. P. Nicorovici, and D. Maystre, "Enhanced SPR sensitivity using periodic metallic structures," *Opt. Express*, vol. 15, no. 13, pp. 8163–8169, Jun. 2007.
[8] T. W. Ebbesen, H. J. Lezec, H. F. Ghaemi, T. Thio, and P. A. Wolff, "Extraordinary optical transmission through sub-wavelength hole arrays," *Nature*, vol. 391, no. 6668, pp. 667–669, Feb. 1998.
[9] H. F. Ghaemi, T. Thio, D. E. Grupp, T. W. Ebbesen, and H. J. Lezec, "Surface plasmons enhance optical transmission through subwavelength holes," *Phys. Rev. B, Condens. Matter*, vol. 58, no. 11, pp. 6779–6782, Sep. 1998.
[10] A. G. Brolo, R. Gordon, B. Leathem, and K. L. Kavanagh, "Surface plasmon sensor based on the enhanced light transmission through arrays of nanoholes in gold films," *Langmuir*, vol. 20, no. 12, pp. 4813–4815, Jun. 2004.
[11] M. E. Stewart, C. R. Anderton, L. B. Thompson, J. Maria, S. K. Gray, J. A. Rogers, and R. G. Nuzzo, "Nanostructured plasmonic sensors," *Chem. Rev.*, vol. 108, no. 2, pp. 494–521, Feb. 2008.
[12] J. M. McMahon, J. Henzie, T. W. Odom, G. C. Schatz, and S. K. Gray, "Tailoring the sensing capabilities of nanohole arrays in gold films with Rayleigh anomaly surface plasmon polaritons," *Opt. Express*, vol. 15, no. 26, pp. 18 119–18 129, Dec. 2007.
[13] J. A. Maynard, N. C. Lindquist, J. N. Sutherland, A. Lesuffleur, A. E. Warrington, M. Rodriguez, and S.-H. Oh, "Next generation SPR technology of membrane-bound proteins for ligand screening and biomarker discovery," *Biotechnol. J.*, vol. 4, no. 11, pp. 1542–1558, Nov. 2009.
[14] K. A. Tetz, L. Pang, and Y. Fainman, "High-resolution surface plasmon resonance sensor based on linewidth optimized nanohole array transmittance," *Opt. Lett.*, vol. 31, no. 10, pp. 1528–1530, May 2006.
[15] G. M. Hwang, L. Pang, E. H. Mullen, and Y. Fainman, "Plasmonic sensing of biological analytes through nanoholes," *IEEE Sensors J.*, vol. 8, no. 12, pp. 2074–2079, Dec. 2008.
[16] A. Lesuffleur, H. Im, N. C. Lindquist, and S. H. Oh, "Periodic nanohole arrays with shape-enhanced plasmon resonance as real-time biosensors," *Appl. Phys. Lett.*, vol. 90, no. 24, pp. 243110-1–243110-3, Jun. 2007.
[17] P. R. H. Stark, A. E. Halleck, and D. N. Larson, "Short order nanohole arrays in metals for highly sensitive probing of local indices of refraction as the basis for highly multiplexed biosensor technology," *Methods*, vol. 37, no. 1, pp. 37–47, Sep. 2005.
[18] A. A. Yanik, M. Huang, A. Artar, T. Y. Chang, and H. Altug, "Integrated nanoplasmonic-nanofluidic biosensors with targeted delivery of analytes," *Appl. Phys. Lett.*, vol. 96, no. 2, pp. 021101-1–021101-3, Jan. 2010.
[19] J. C. Yang, J. Ji, J. M. Hogle, and D. N. Larson, "Multiplexed plasmonic sensing based on small dimension nanohole arrays and intensity interrogation," *Biosens. Bioelectron.*, vol. 24, no. 8, pp. 2334–2338, Apr. 2009.
[20] K. L. Lee, S. H. Wu, and P. K. Wei, "Intensity sensitivity of gold nanostructures and its application for high-throughput biosensing," *Opt. Express*, vol. 17, no. 25, pp. 23 104–23 113, Dec. 2009.
[21] J. C. Sharpe, J. S. Mitchell, L. Ling, N. Sedoglavich, and R. J. Blaikie, "Gold nanohole array substrates and immunobiosensors," *Anal. Chem.*, vol. 80, no. 6, pp. 2244–2249, 2008.
[22] J. F. Masson, M. P. M. Methot, and L. S. Live, "Nanohole arrays in chemical analysis: Manufacturing methods and applications," *Analyst*, vol. 135, no. 7, pp. 1483–1489, 2010.
[23] E. Stenberg, B. Persson, H. Roos, and C. Urbaniczky, "Quantitative determination of surface concentration of protein with surface plasmon resonance using radiolabeled proteins," *J. Colloid Interface Sci.*, vol. 143, no. 2, pp. 513–526, May 1991.
[24] M. Vala, K. Chadt, M. Piliarik, and J. Homola, "High-performance compact SPR sensor for multi-analyte sensing," *Sens. Actuators B, Chem.*, vol. 148, no. 2, pp. 554–549, Jul. 2010.
[25] T. M. Chinowsky, L. S. Jung, and S. S. Yee, "Optimal linear data analysis for surface plasmon resonance biosensors," *Sens. Actuators B, Chem.*, vol. 54, no. 1/2, pp. 89–97, Jan. 1999.
[26] P. Tobiška and J. Homola, "Advanced data processing for SPR biosensors," *Sens. Actuators B, Chem.*, vol. 107, no. 1, pp. 162–169, May 2005.
[27] K. S. Johnston, K. S. Booksh, T. M. Chinowsky, and S. S. Yee, "Performance comparison between high and low resolution spectrophotometers used in a white light surface plasmon resonance sensor," *Sens. Actuators B, Chem.*, vol. 54, no. 1/2, pp. 80–88, Jan. 1999.
[28] M. E. Stewart, J. Tao, J. Maria, S. K. Gray, and J. A. Rogers, "Multispectral thin film biosensing and quantitative imaging using 3D plasmonic crystals," *Anal. Chem.*, vol. 81, no. 15, pp. 5980–5989, Aug. 2009.
[29] Y. L. Yeh, "Real-time measurement of glucose concentration and average refractive index using a laser interferometer," *Opt. Lasers Eng.*, vol. 46, no. 9, pp. 666–670, Sep. 2008.
[30] M. H. Lee, H. Gao, J. Henzie, and T. W. Odom, "Microscale arrays of nanoscale holes," *Small*, vol. 3, no. 12, pp. 2029–2033, Dec. 2007.
[31] D. Lepage, A. Jiménez, D. Carrier, J. Beauvais, and J. J. Dubowski, "Hyperspectral imaging of diffracted surface plasmons," *Opt. Express*, vol. 18, no. 26, pp. 27 327–27 335, Dec. 2010.